AJNR

# Comparison of Two Superparamagnetic Viral-Sized Iron Oxide Particles Ferumoxides and Ferumoxtran-10 with a Gadolinium Chelate in Imaging Intracranial Tumors

Peter Varallyay, Gary Nesbit, Leslie L. Muldoon, Randal R. Nixon, Johnny Delashaw, James I. Cohen, Annie Petrillo, Doris Rink and Edward A. Neuwelt



*AJNR Am J Neuroradiol* 2002, 23 (4) 510-519
http://www.ajnr.org/content/23/4/510

*AJNR Am J Neuroradiol* 23:510–519, April 2002

# Comparison of Two Superparamagnetic Viral-Sized Iron Oxide Particles Ferumoxides and Ferumoxtran-10 with a Gadolinium Chelate in Imaging Intracranial Tumors

Peter Varallyay, Gary Nesbit, Leslie L. Muldoon, Randal R. Nixon, Johnny Delashaw, James I. Cohen, Annie Petrillo, Doris Rink, and Edward A. Neuwelt

***BACKGROUND AND PURPOSE:*** **Ultrasmall superparamagnetic iron oxide particles result in shortening of T1 and T2 relaxation time constants and can be used as MR contrast agents. We tested four hypotheses by evaluating MR images of intracranial tumors after infusion of two iron oxide agents in comparison with a gadolinium chelate: 1) Ferumoxtran in contrast to ferumoxides can be used as an intravenous MR contrast agent in intracranial tumors; 2) ferumoxtran enhancement, albeit delayed, is similar to gadolinium enhancement; 3) ferumoxtran-enhanced MR images in contrast to gadolinium-enhanced MR images may be compared with histologic specimens showing the cellular location of iron oxide particles; 4) ferumoxtran can serve as a model for viral vector delivery.**

***METHODS:*** **In 20 patients, ferumoxides and ferumoxtran were intravenously administered at recommended clinical doses. MR imaging was performed 30 minutes and 4 hours after ferumoxides infusion (n = 3), whereas ferumoxtran-enhanced MR imaging (n = 17) was performed 6 and 24 hours after infusion in the first five patients and 24 hours after infusion in the remaining 12. MR sequences were spin-echo (SE) T1-weighted, fast SE T2- and proton density–weighted, gradient-recalled-echo T2*-weighted, and, in four cases, echo-planar T2-weighted sequences. Representative regions of interest were chosen on pre- and postcontrast images to compare each sequence and signal intensity.**

***RESULTS:*** **Despite some degree of gadolinium enhancement in all tumors, no significant T1 or T2 signal intensity changes were seen after ferumoxides administration at either examination time. Fifteen of 17 patients given ferumoxtrans had T1 and/or T2 shortening consistent with iron penetration into tumor. Histologic examination revealed minimal iron staining of the tumor with strong staining at the periphery of the tumors.**

***CONCLUSION:*** **1) Ferumoxtran can be used as an intravenous MR contrast agent in intracranial tumors, mostly malignant tumors. 2) Enhancement with ferumoxtran is comparable to but more variable than that with the gadolinium chelate. 3) Histologic examination showed a distribution of ferumoxtran particles similar to that on MR images, but at histology the cellular uptake was primarily by parenchymal cells at the tumor margin. 4) Ferumoxtran may be used as a model for viral vector delivery in malignant brain tumors.**

Ultrasmall superparamagnetic iron oxide (USPIO) particles have been under extensive research for the past decade as MR imaging contrast agents. They have proved useful in several applications including imaging of the gastrointestinal system, liver (1–4), and spleen (5) and may also help[1] in differentiating between malignant and benign lymph nodes (6–8). Because USPIO particles may also serve as a blood-

Received August 20, 2001; accepted after revision January 14, 2002.

From the Departments of Neurology (P.V., L.L.M., A.P., D.R., E.A.N.), Radiology (P.V., G.N.), Neurosurgery (J.D., E.A.N.), Cell and Developmental Biology (L.L.M.), Pathology (R.R.N.), and Otolaryngology (J.I.C.), Oregon Health and Science University, Portland, Oregon.

Supported by a Veterans Administration merit review grant and by grants NS34608, NS33618 and CA31770 from the National Institutes of Health.

Address reprint requests to Edward A. Neuwelt, MD, Oregon Health and Science University, 3181 SW Sam Jackson Park Rd, L603, Portland, OR 97201.

pool agent, they may be used for MR angiography and perfusion imaging of the brain and heart (9–11).

Depending on their structure, iron oxide particles have different intravascular half-lives and are variably taken up in the reticuloendothelial system. In reactive brain lesions, they can also be found in the vascular endothelium and in the perivascular space (12). Studies have also shown promise with the use of USPIO particles in detecting active inflammatory or demyelinating lesions because of iron uptake in perivascular macrophages (12–14). In addition, iron oxide particles can be detected in the central nervous system in neurons after either direct inoculation or blood-brain barrier (BBB) disruption (15, 16), as well as in malignant glial tumors after intravenous administration (17–20) and in cell lines in vitro (21). In other studies, USPIO particles have been used to assess the variables in maximizing the volume of distribution after direct interstitial infusion by convection in a rat model (22), as well as to demonstrate antibody targeted delivery (23). USPIO particles may be identified at the light and electron microscopic levels, allowing evaluation of their exact location within tissues (15, 16), unlike other central nervous system MR imaging agents.

Two iron oxide agents were examined in this study. Ferumoxides (Feridex IV; Advanced Magnetics, Cambridge, MA), which is approved by the U.S. Food and Drug Administration (FDA) for liver imaging, has a mean particle size of 58.5 nm ± 185.8 (volume weighted). The particle cores are aggregates of iron crystals incompletely coated with dextran and have a large size distribution as well as irregularity in shape (24). Ferumoxides tends to be rapidly opsonized and taken up by the reticuloendothelial system, and therefore it has a short plasma half-life of 8–30 minutes. Ferumoxtran-10 (Combidex; Advanced Magnetics) has a mean particle size of 29.5 nm ± 23.1 (volume weighted), consists of monocrystalline cores, is more uniform in shape and size, and is completely coated with a thicker dextran layer (24). Ferumoxtran-10 has a plasma half-life of 25–30 hours, therefore the organ uptake duration is much longer than that with ferumoxides.

This study was designed to answer the following hypotheses: 1) ferumoxtran, in contrast to ferumoxides, may be used as an intravenous contrast agent for MR imaging of intracranial tumors; 2) ferumoxtran enhancement, albeit delayed, is similar to enhancement with a gadolinium-based contrast agent; 3) ferumoxtran-enhanced MR images, in contrast to gadolinium-enhanced MR images, may be compared with histologic specimens showing the location of the iron oxide particles at the cellular level in tumors; and 4) ferumoxtran may serve as a model for viral vector delivery.

## Methods

Twenty patients (age range, 30–66 years; mean age, 47.2 years) with primary and metastatic intracranial tumors were enrolled in this FDA- and institutional review board–approved study from December 1999 to December 2001. Six patients were randomly assigned to receive either ferumoxides or ferumoxtran before a lack of substantial iron accumulation was found on MR images after ferumoxides infusion (Table). At that point, ferumoxtran was used exclusively. Written informed consent was obtained from each patient. All patients underwent MR imaging with a gadolinium-based contrast agent (Omniscan [gadodiamide]; Nycomed Imaging, Oslo, Norway) at least 24 hours before but no more than 28 days before iron infusion.

Ferumoxides was administered intravenously in three patients at the recommended clinical dose of 0.56 mg of iron per kilogram of body weight, and MR imaging was performed 30 minutes and 4 hours after infusion. Ferumoxtran was administered intravenously, under FDA-approved Investigational New Drug approval, in 17 patients at a dose of 2.6 mg Fe/kg, diluted in 50 mL of normal saline, infused at 4 mL/min. Because of the increased intravascular half-life, MR images were obtained 6 hours and 24 hours after the infusion of ferumoxtran in the first five patients; the remaining 12 patients underwent MR imaging only at 24 hours because the signal intensity changes were stronger and extended into a larger area at 24 hours.

All patients underwent MR imaging with spin-echo (SE) T1-weighted, fast SE T2-weighted, fast SE proton density–weighted, and gradient-recalled-echo (GRE) T2*-weighted sequences; one patient underwent echo-planar SE T2-weighted imaging; one patient underwent echo-planar GRE T2*-weighted imaging; and one patient underwent both echo-planar SE T2-weighted and echo-planar GRE T2*-weighted imaging. Multiplanar images were obtained with a 1.5-T superconducting magnet (Gyroscan, Philips, Best, the Netherlands; or Horizon LX, GE Medical Systems, Milwaukee, WI) with a 23-cm field of view. SE T1-weighted images were obtained with 500/13/2 (TR/TE/NEX), fast SE T2-weighted images were acquired with 3000/95/2, and fast SE proton density–weighted images were obtained with 2500/13/2. GRE T2*-weighted images were acquired with 750/23/2, flip angle 10°; multishot (echo-planar imaging factor 3) echo-planar GRE T2*-weighted images were obtained with 750/23/2, flip angle 10°; and echo-planar SE T2-weighted images were obtained with 4880/90/2 (echo-planar imaging factor 11). The matrix size was 256 × 192, section thickness was 3 mm, and intersection gap was 1 mm.

For quantitative analysis, the two patients with nasopharyngeal carcinoma (patients 10 and 11) who received ferumoxtran were excluded because they had only minimal intracranial spread, with mandibular nerve and dural involvement in the region of the foramen ovale. To compare ferumoxtran accumulation with gadolinium enhancement in the remaining 15 patients, representative regions of interest (ROIs) were chosen on the ferumoxtran-enhanced SE T1-weighted images in areas of maximal, minimal, and absent ferumoxtran enhancement and, for reference, in an area of normal-appearing brain. By using the pre–ferumoxtran-enhanced fast SE T2-weighted and the gadolinium-enhanced SE T1-weighted images, an ROI was also obtained in the area of T2 signal intensity abnormality that surrounded the gadolinium-enhancing tumor (ie, brain around the enhancing tumor). The same areas of ROI were carefully applied on each of the following images in the 15 patients: pre–gadolinium-enhanced SE T1-weighted, gadolinium-enhanced SE T1-weighted, ferumoxtran-enhanced SE T1-weighted, pre–ferumoxtran-enhanced fast SE T2-weighted, ferumoxtran-enhanced fast SE T2-weighted, and ferumoxtran-enhanced GRE T2*-weighted. Most patients were enrolled in the study after undergoing routine brain MR imaging with and without the gadolinium-based contrast agent; this did not include a GRE T2*-weighted series. However, two of the 15 patients underwent pre–ferumoxtran-enhanced GRE T2*-weighted imaging; thus, on these images the same areas of ROI were obtained. One patient underwent ferumoxtran-enhanced echo-planar GRE T2*-weighted imaging, another patient underwent ferumoxtran-enhanced echo-

**Demographics and imaging results**

| Patient No./ Sex/Age (y) | Histologic Diagnosis | Tumor Location | USPIO | Iron Uptake | T1 Signal Intensity Change | T2 Signal Intensity Change |
|---|---|---|---|---|---|---|
| 1/F/48 | Metastatic large cell carcinoma | Cerebellum | Ferumoxides | − | − | − |
| 2/M/46 | Anaplastic oligodendraglioma | R temporoparietal | Ferumoxides | +* | + | − |
| 3/F/53 | Meningioma | L frontal | Ferumoxides | − | − | − |
| 4/M/54 | Gliblastoma multiforme | L thalamus, parietal | Ferumoxtran-10 | + | + | + |
| 5/M/55 | Anaplastic oligodendraglioma | L temporal | Ferumoxtran-10 | +† | + | + |
| 6/M/54 | Oligodendroglioma | L frontotemporal | Ferumoxtran-10 | − | − | − |
| 7/F/47 | Hamartoma | L temporal | Ferumoxtran-10 | +* | + | − |
| 8/F/30 | Medulloblastoma | Cerebellum | Ferumoxtran-10 | +† | + | + |
| 9/M/58 | Anaplastic oligodendraglioma | R temporoparietal | Ferumoxtran-10 | +† | + | + |
| 10/M/55 | Squamous cell carcinoma | Nasopharynx with skull base invasion | Ferumoxtran-10 | + | + | + |
| 11/M/50 | Squamous cell carcinoma | Nasopharynx with skull base invasion | Ferumoxtran-10 | + | + | + |
| 12/F/42 | Meningioma | L petroclival | Ferumoxtran-10 | +† | + | + |
| 13/M/57 | Oligodendroglioma | R parietal | Ferumoxtran-10 | − | − | − |
| 14/M/55 | Anaplastic glioma | L temporal | Ferumoxtran-10 | +* | + | − |
| 15/F/54 | Glioblastoma multiforme | R temporoparietal | Ferumoxtran-10 | + | + | + |
| 16/F/66 | Glioblastoma multiforme | R frontal | Ferumoxtran-10 | +† | + | + |
| 17/F/57 | Anaplastic oligodendraglioma | R frontal | Ferumoxtran-10 | +† | + | + |
| 18/M/54 | Pituitary adenoma | Intra- and suprasellar | Ferumoxtran-10 | + | + | + |
| 19/M/39 | Glioblastoma multiforme | L fronto-opercular | Ferumoxtran-10 | + | + | + |
| 20/M/46 | Anaplastic oligodendraglioma | R posterior temporal | Ferumoxtran-10 | +† | + | + |

Note.—L indicates left; R, right; +, yes; −, no.

* Iron accumulation was only minimal compared with gadolinium enhancement.

† Ferumoxtran enhancement as measured with ROI (see Methods) was regionally more prominent than gadolinium enhancement.

planar SE T2-weighted imaging, and in a third patient both ferumoxtran-enhanced echo-planar SE T2-weighted and echo-planar GRE T2*-weighted sequences were performed.

Signal intensities were measured in each ROI, and the signal intensity values were normalized to normal brain for each sequence, making a ratio by dividing the signal intensity value in a specific ROI with the signal intensity value of the normal-appearing brain area. The normalized quantitative signal intensity values of the different ROIs for each sequence were analyzed and compared, and the level of significance was determined by using a paired-samples *t* test. A *P* value of less than .05 was considered to indicate a statistically significant difference.

Minimal signal intensity change was detected in only one of the patients receiving ferumoxides; therefore, similar quantitative measurements were not made in the three patients who received ferumoxides.

Two neuroradiologists (P.V., G.N.) and a neurosurgeon (E.A.N.) reviewed the images, and a consensus was made if there were different opinions regarding where to place the specific ROIs. The above-described method ruled out the possibility for evaluation to be blinded for gadolinium-enhanced images and ferumoxtran- or ferumoxides-enhanced images, because the ROIs had to be chosen in areas of ferumoxtran enhancement.

Biopsy specimens were immersion-fixed in neutral buffered formalin for at least 24–48 hours, then imbedded in egg yolk-gelatin. Serial vibratome sections (100 $\mu$m) from throughout the biopsy specimens were assessed for iron localization. Histochemical staining for iron was performed by using the diaminobenzidine (DAB)–enhanced Perls stain, as described previously (15, 16); sections were counterstained with hematoxylin.

## Results

Despite the presence of gadolinium enhancement in all tumors, no sign of iron penetration into tumor (ie, T1 or T2 signal intensity changes) was seen in two of the three patients at either examination time after the intravenous administration of ferumoxides with the maximum clinically approved dose. One patient who received ferumoxides had only a tiny area of increased T1 signal intensity (much fainter and smaller than the gadolinium-enhancing area) without detectable T2 signal intensity change, consistent with a very small amount of iron accumulation (Fig 1).

Fifteen of the 17 patients who received ferumoxtran had T1 and/or T2 shortening consistent with iron accumulation in the tumor (Figs 2–4). The hyperintense T1 signal intensity changes were readily detectable, and the hypointense fast SE T2 and GRE T2* signal intensity changes were modest and more variable. The signal intensity changes were stronger and extended into a larger area on the 24-hour ferumoxtran-enhanced images compared with the 6-hour study (Fig 2).

In general, 13 of the 15 brain tumors had signal intensity changes in the approximate region where gadolinium enhancement was seen (Figs 2–4), but three of the 13 patients (patients 9, 17, and 20) had ferumoxtran enhancement even in areas of no gadolinium enhancement (Fig 3, Table). Four of the thirteen patients (patients 8, 12, 16, and 17) had higher normalized T1 signal intensity with ferumoxtran than with the gadolinium chelate in the maximal ROI, and four patients (patients 5, 8, 16, and 17) showed higher normalized T1 signal intensity with ferumoxtran than with the gadolinium chelate in the minimal ROI (Table). Only the two low-grade oligodendrogliomas (Fig

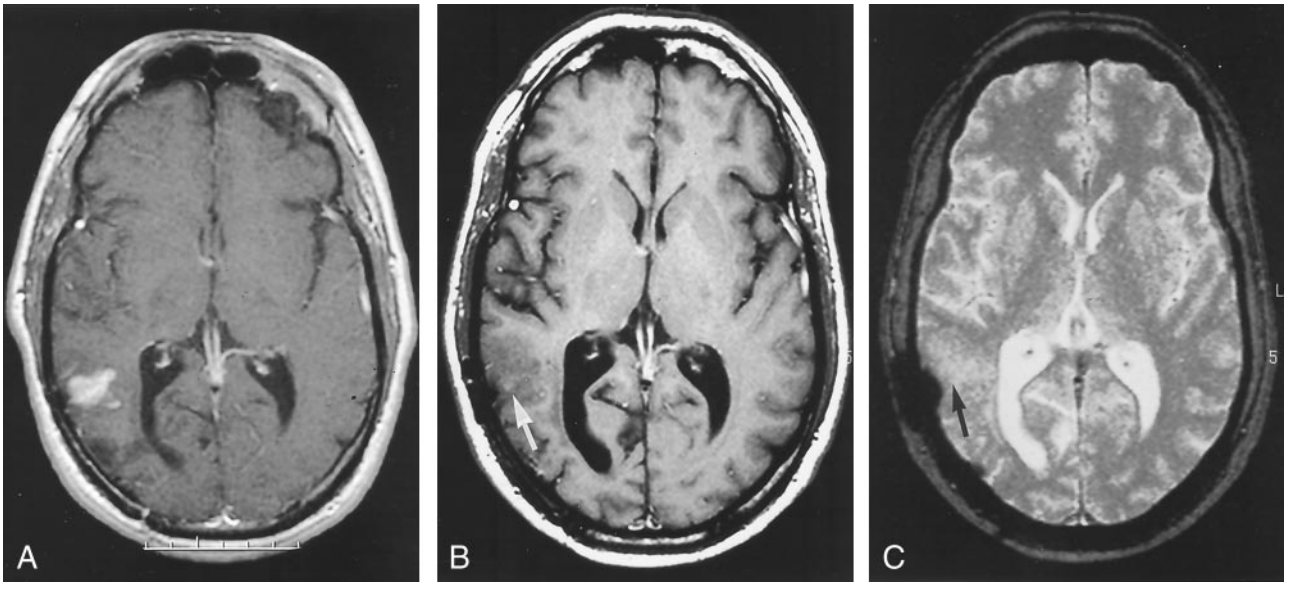


FIG 1. Patient 2 with anaplastic oligodendroglioma.
*A*, Gadolinium-enhanced SE T1-weighted image shows an intensely enhancing tumor nodule in the posterior right temporal lobe.
*B* and *C*, Four hours after ferumoxides infusion, SE T1-weighted image (*B*) shows only a tiny area of increased signal intensity (*arrow*), whereas the GRE T2*-weighted image (*C*) demonstrates no decreased signal intensity (*arrow*). The rounded hypointense lateral region in *C* is from a craniotomy plate.

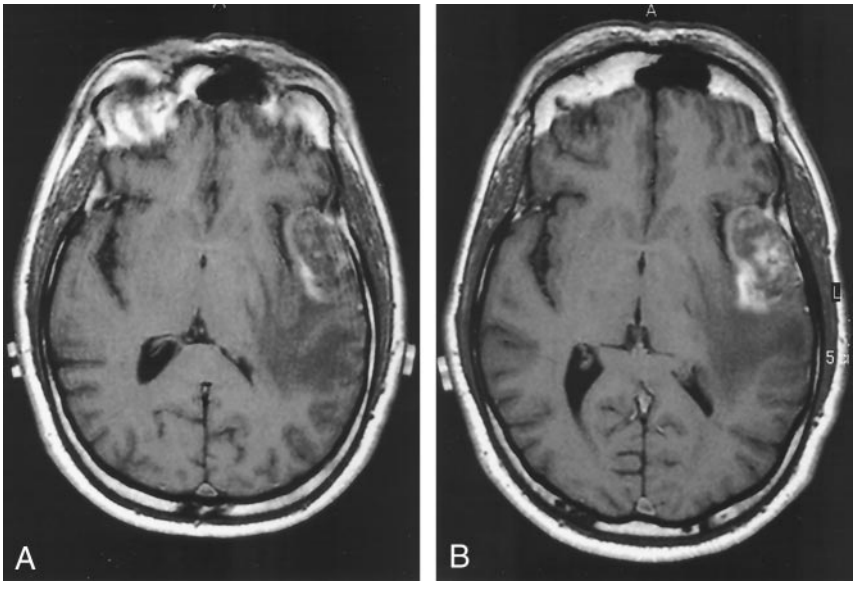


FIG 2. Patient 5 with anaplastic oligodendroglioma.
*A* and *B*, SE T1-weighted images obtained 6 hours (*A*) and 24 hours (*B*) after ferumoxtran infusion show progressive peripheral and patchy central enhancement in the left temporal tumor.

5) demonstrated no signal intensity changes (neither T1 nor T2) with ferumoxtran (Table). The two nasopharyngeal carcinomas also revealed T1 and T2 shortening in the areas of abnormal gadolinium enhancement in the parapharyngeal area and in the region of the involved skull base. The venous structures had variable T1 signal hyperintensity and persistent T2 hypointensity due to the persistent blood concentration of ferumoxtran secondary to its long plasma half-life.

The T1 and T2 shortening effects of ferumoxtran were obvious (Figs 6 and 7) with progressive accumulation of the USPIOs from 6 to 24 hours ($P < .05$). In the area of maximal ferumoxtran enhancement, the degree of enhancement was similar and significant ($P < .001$) with ferumoxtran and gadolinium, with no significant difference between the ferumoxtran-enhanced SE T1 and gadolinium-enhanced SE T1 signal intensities (Fig 6). In the area of minimal ferumoxtran enhancement, both gadolinium ($P < .001$) and ferumoxtran ($P < .005$) demonstrated significant enhancement compared with the precontrast images, but gadolinium-enhanced SE T1-weighted images showed higher signal intensity compared with that on ferumoxtran-enhanced SE T1-weighted images ($P < .05$) (Fig 6). In the area of maximal and minimal ferumoxtran enhancement, significant decrease ($P < .001$, $P < .01$, respectively) in signal intensity was seen between the precontrast and ferumoxtran-enhanced fast SE T2-weighted images (Fig 7).

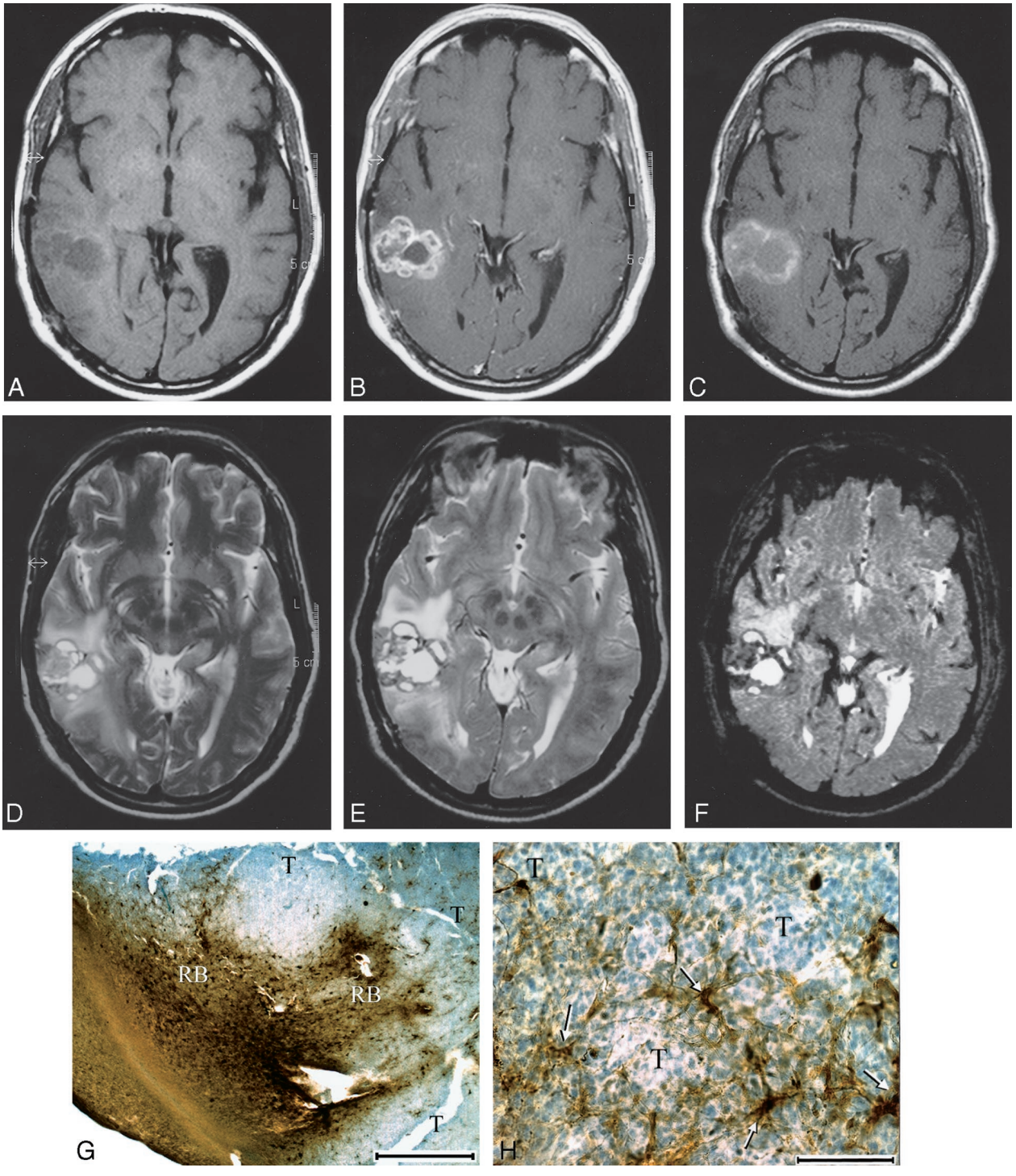


FIG 3. Patient 9 with anaplastic oligodendroglioma.

*A* and *B*, Nonenhanced (*A*) and gadolinium-enhanced (*B*) SE T1-weighted images of the right temporal tumor. The gadolinium-enhanced image shows evidence of strong, lobulated peripheral enhancement with a central nonenhancing zone.

*C*, At 24 hours after ferumoxtran infusion, SE T1-weighted image demonstrates marked high signal intensity in a similar distribution but with less peripheral lobulation compared with the gadolinium-enhanced image. Also note that the non–gadolinium-enhancing central zone became isointense to white matter, suggesting some ferumoxtran accumulation.

*D–F*, Fast SE T2-weighted image obtained before ferumoxtran infusion (*D*) and fast SE T2-weighted (*E*) and GRE T2*-weighted (*F*) images obtained 24 hours after ferumoxtran infusion show a heterogeneous tumor mass with peripheral decreased signal intensity that is more prominent on the GRE T2*-weighted image. The distribution of the low-signal-intensity areas is similar to that of the high-signal-intensity areas on the SE T1-weighted image in *C*.

*G* and *H*, Photomicrographs from histologic staining for iron (DAB-enhanced Perls stain). In *G* (original magnification ×7.5; bar indicates 1 mm), tumor (*T*) and reactive brain interface (*RB*) show the intense staining for iron at the periphery of the tumor. In *H* (original magnification ×100; bar indicates 0.1 mm), cellular iron staining at the tumor–reactive brain interface shows iron uptake by the parenchymal cells with fibrillar processes (*arrows*) rather than by the round tumor cells (*T*).

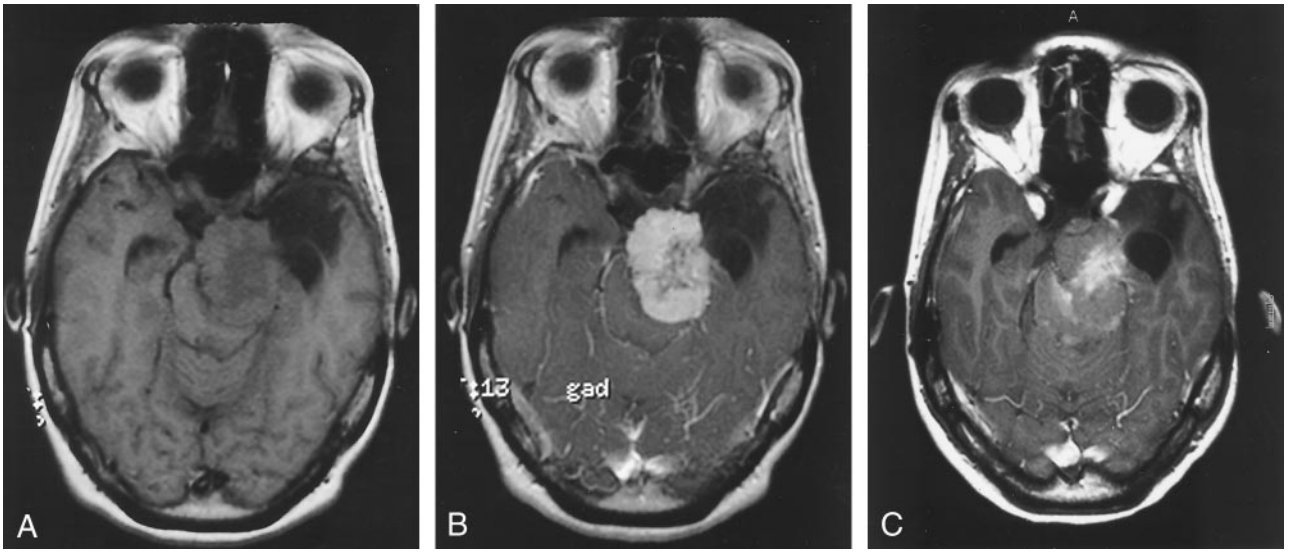


FIG 4. Patient 12 with meningioma, after radiation therapy.

*A* and *B,* Nonenhanced (*A*) and gadolinium-enhanced (*B*) SE T1-weighted images. The image in *B* shows evidence of strong enhancement, except in the central region.

*C*, At 24 hours after ferumoxtran infusion, SE T1-weighted image shows strong ferumoxtran enhancement in the less gadolinium-enhancing central region and only minimal ferumoxtran enhancement in the surrounding intensely gadolinium-enhancing portion.

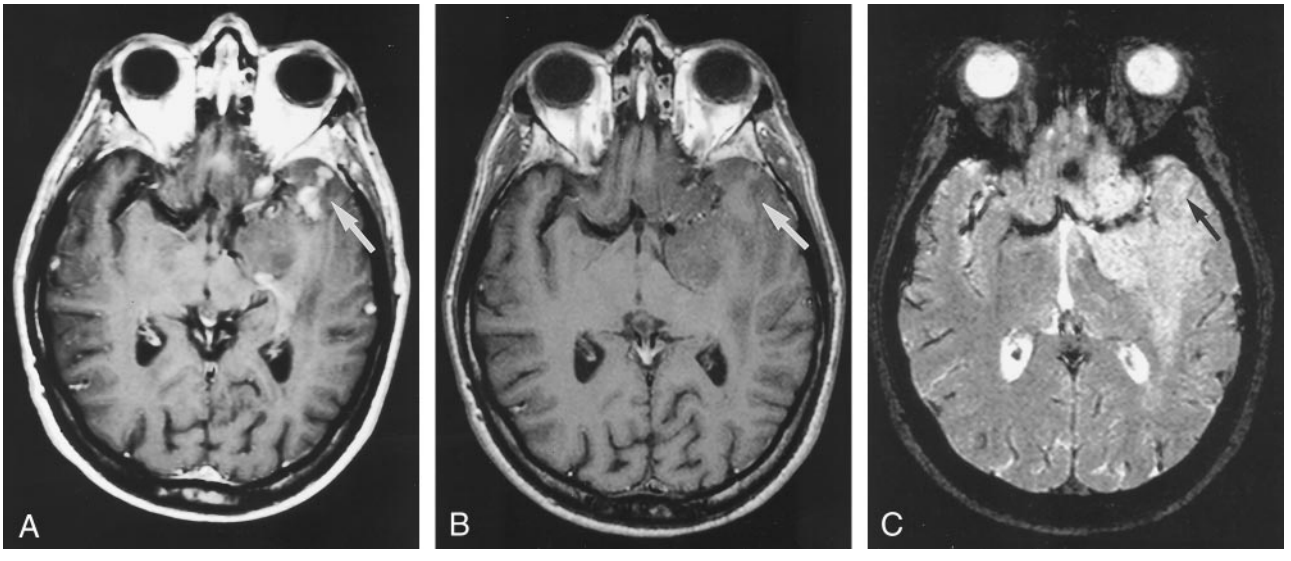


FIG 5. Patient 6 with oligodendroglioma.

*A*, Gadolinium-enhanced SE T1-weighted image shows a large left frontotemporal mass (arrow) with only small areas of enhancement in its anterior aspect.

*B* and *C*, At 24 hours after ferumoxtran infusion, SE T1-weighted (*B*) and GRE T2*-weighted (*C*) images demonstrate no signal intensity changes (*arrow*), indicating no accumulation of iron.

The lack of pre–ferumoxtran-enhanced GRE T2*-weighted images in all but two patients did not allow us to statistically compare the ferumoxtran-enhanced GRE T2* signal intensities with the pre–ferumoxtran-enhanced GRE T2* signal intensities. However, in the minimal ferumoxtran-enhancing region and brain around enhancing tumor, there were significantly lower normalized signal intensities ($P < .005$, $P < .05$, respectively) on GRE T2*-weighted images than on fast SE T2-weighted images, with easier visual detectability of T2 shortening on GRE T2*-weighted images (Fig 7). In the two patients who also had nonenhanced and ferumoxtran-enhanced GRE T2*-weighted images, we could measure the percentage of signal intensity decrease, which was compared with the fast SE T2 signal intensity decrease. The first patient showed 77% signal intensity decrease on GRE T2*-weighted images and 65% signal intensity decrease on fast SE T2-weighted images in the maximal ferumoxtran-enhancing ROI, and 55% signal intensity decrease on GRE T2*-weighted images and 10% signal intensity decrease on fast SE T2-weighted images in the minimal ferumoxtran-enhancing ROI. The second patient demonstrated 62%, 38%, 30%, and 13.5% signal intensity decrease, respectively. The four ferumoxtran-enhanced echo-planar imaging studies revealed no

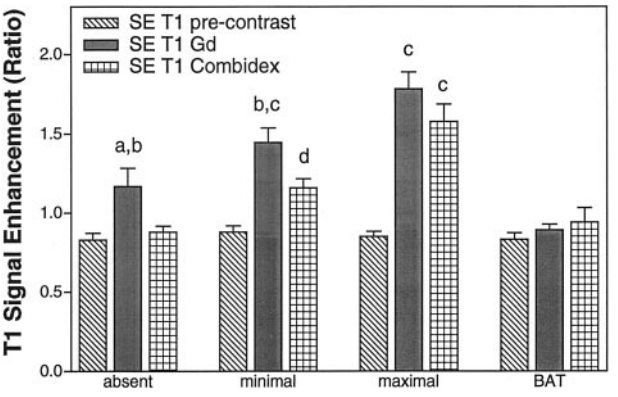


FIG 6. Quantitation of SE T1-weighted MR images. Normalized mean SE T1 signal intensity values with standard mean error in areas of absent, minimal, and maximal ferumoxtran enhancement in the tumor as well as in brain around tumor (*BAT*) (n = 15 patients). *a* indicates $P < .05$ for gadolinium (*Gd*) enhancement compared with precontrast images; *b*, $P < .05$ for gadolinium enhancement compared with ferumoxtran (*Combidex*) enhancement; *c*, $P < .001$ compared with precontrast image; *d*, $P < .005$ compared with precontrast images.

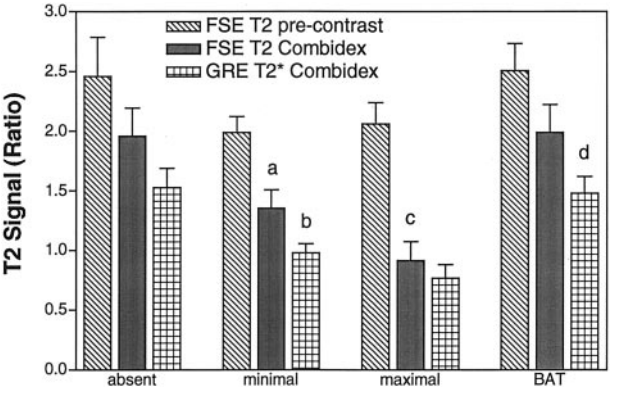


FIG 7. Quantitation of fast SE T2-weighted and GRE T2*-weighted MR images. Normalized mean T2 signal intensity values with standard mean error in areas of absent, minimal, and maximal ferumoxtran enhancement in the tumor as well as in brain around tumor (*BAT*) (n = 15 patients). *a* indicates $P < .01$ compared with the precontrast fast SE (*FSE*) T2-weighted images; *b*, $P < .005$ comparing ferumoxtran (*Combidex*)-enhanced GRE T2*-weighted images with ferumoxtran-enhanced fast SE T2-weighted images; *c*, $P < .001$ compared with precontrast fast SE T2-weighted images; *d*, $P < .05$ comparing ferumoxtran-enhanced GRE T2*-weighted images with ferumoxtran-enhanced fast SE T2-weighted images.

clear signal intensity difference between the echo-planar GRE T2*-weighted and echo-planar SE T2-weighted images versus GRE T2*-weighted images, and the susceptibility artifacts and geometric distortion were more prominent with the echo-planar sequences.

Biopsy specimens from a patient given ferumoxtran (patient 9, Table) were stained for iron histochemistry (Fig 3G and H). The close-packed blue nuclear staining indicates the area of tumor; only scattered cells demonstrated iron staining. Most of the staining within the tumor was in cells with fine fibrillar processes, suggesting an astrocytic or microglial derivation. Staining was much more dense at the periphery of the tumor at the brain interface. At higher magnification, staining appeared to be in both neurons and astrocytes. The pattern of histologic staining (Fig 3G and H) correlated quite well with MR changes (Fig 3A–F), that is, marked signal intensity changes and iron staining peripherally with minimal changes centrally either at MR imaging or histologic examination.

## Discussion

Lack of, or only minimal, tumor signal intensity changes with ferumoxides in this study may be explained first by the structure of this iron oxide particle. The thin (3.3 nm) and incomplete dextran coating results in rapid protein- and membrane-binding (opsonization) when in circulation and thus a short plasma half-life. This hypothesis is also supported by the fact that there were no detectable signal intensity changes even in the case of the meningioma (patient 3), which does not have a BBB and is highly vascularized, and yet it did not show iron accumulation. Other features such as its relatively larger particle size and the large variety in size (compared with ferumoxtran) as well as its shape irregularity may also contribute to ferumoxides being unable or only minimally able to cross the incompetent BBB. Lack of or only minimal tumor signal intensity changes on ferumoxides-enhanced images compared with gadolinium-enhanced images in our initial three patients led us to discontinue the use of ferumoxides in our clinical studies, although it theoretically may better represent viruses that are also easily opsonized and are taken up by the immune system cells. The almost five-fold smaller dose of ferumoxides than ferumoxtran might also play a role in the minimal or no enhancement seen with ferumoxides, but the administered doses were the largest clinically approved doses we could use.

Ferumoxtran showed signal intensity changes in most of the gadolinium-enhancing regions, consistent with USPIO accumulation in the tumors. Thicker (8–12 nm) and complete dextran coating of this iron oxide particle prevents it from reacting with plasma proteins and membranes. The somewhat smaller and more uniform size, compared with that of ferumoxides, may improve the ability of the ferumoxtran iron oxide particles to cross the damaged BBB (endothelial junctions and basement membrane) (15). A long plasma half-life (25–30 hours) may create enough time for these iron oxide particles to "search for" the most leaky areas of the damaged BBB, and because of their uniform size, more iron oxide particle may cross the BBB resulting in good detectability with MR imaging.

In brain, signal intensity changes versus iron oxide concentration has been studied in detail (15). Whereas iron uptake results in continuous T2 shortening with higher concentrations (ie, decreased signal intensity on T2-weighted images), the T1 shortening effect (ie, increased signal intensity on T1-weighted images) peaks at lower concentrations and then decreases with higher concentrations, and in cases of very high concentrations of iron, slight decreased signal intensity can be found. Iron oxide particles are

much more effective in MR relaxation than their more common paramagnetic (gadolinium) counterpart (24) and can be detected in vivo at lower concentrations down to 1 $\mu$g (15, 16). In the current series, ferumoxtran resulted in increased T1 and decreased T2 signal intensity; thus, at the applied doses, the iron accumulation is not concentrated enough to cause decreased T1 signal intensity.

The findings from this study corroborate the observation of Enochs et al (17) that different pathologic tissues can show different enhancement with distinct classes of MR contrast agents. It is widely accepted that BBB breakdown may be variable not only in the case of different histologic types of tumors but also within one tumor mass (25–27). The question remains of the mechanism and the necessary conditions for enhancement by different contrast agents other than gadolinium-based contrast agents. It is reasonable to assume that even if the BBB becomes incompetent for low-molecular-weight gadolinium, it does not necessarily mean that it is leaky enough to allow larger sized particles (ferumoxtran) to enter the interstitium (27). Ferumoxtran accumulation (enhancement) may also be related to cell metabolic activity. Studies have shown that metabolically active cells such as malignant glial cells take up the iron oxide particles by endocytosis in vitro (21). Some investigators (17–20) have also demonstrated that this iron uptake by malignant glial cells may also occur in vivo, but according to our animal experiments tumor cell uptake of ferumoxtran in vivo is often poor. Further studies are necessary to determine the exact location of iron particles in the tumor and in adjacent tissues in vivo.

Ferumoxtran enhancement also seems to depend on the amount of parenchymal cells capable of taking up the iron particles. Histologic staining of the tumor and brain around enhancing tumor (Fig 3G and H) from a patient with distinct ferumoxtran enhancement (Fig 3A–F) showed iron uptake by scattered cells within the tumor and strong iron staining at the tumor periphery and brain around enhancing tumor. Although some stained cells may be tumor, as evidenced by small round morphology, most staining is found in cells with fine fibrillar processes with astrocytic morphology. The results suggest that two major phenomena come into play for ferumoxtran enhancement. First is crossing the BBB, allowing passage of ferumoxtran from the intravascular space. Second is the presence of parenchymal cells capable of accumulating the ferumoxtran particles. Absent or minimal ferumoxtran enhancement in areas within tumor that show gadolinium enhancement may thus be due to a variably incompetent BBB for the smaller gadolinium and the larger ferumoxtran molecules and/or a variable presence or ability of the cells that take up iron. Further evaluation of these hypotheses with multiple tumor samples is underway.

Only in the two low-grade oligodendrogliomas (patients 6 and 13, Fig 5) was there no sign of ferumoxtran penetration into the tumor despite the evidence of BBB breakdown by gadolinium enhancement. The hamartoma (patient 7) had only slight ferumoxtran enhancement compared with the more prominent gadolinium enhancement, and this faint ferumoxtran enhancement occurred in the gadolinium-enhancing areas. The difference between gadolinium and ferumoxtran enhancement in these low-grade gliomas (patients 6, 7, and 13) may be the result of the above-described possible mechanisms.

The meningioma (patient 12, Fig 4) demonstrated variable ferumoxtran enhancement despite prominent gadolinium enhancement. This could suggest either variable vascular endothelium barrier much more permeable to the gadolinium chelate than to the larger ferumoxtran, except in its central portion, or the lack of parenchymal cells capable of trapping ferumoxtran. In patient 14, the anaplastic glioma showed just scattered areas of ferumoxtran enhancement within the more homogeneously gadolinium-enhancing tumor. These two cases, in which the patients underwent radiation therapy, suggest that prior radiation may have had an effect on the vascular endothelium, causing endothelial proliferation, and thereby impeded ferumoxtran penetration (28). A large pituitary tumor (patient 18) also showed only modest ferumoxtran enhancement despite excellent gadolinium enhancement, which may be primarily a reflection of only a few cells capable of taking up the iron within the tumor.

The presence of ferumoxtran enhancement in regions of no gadolinium enhancement (patients 9, 17, and 20) may suggest a separate mechanism of passing across the BBB than the intercellular junctions. Patient 20 with anaplastic oligodendroglioma showed significantly increased T1 and decreased T2 signal intensities in the brain around enhancing tumor, where gadolinium enhancement could not be observed at all. Although the time interval between the two images was 26 days and there was mild interval progression both in size of the solid tumor and mass effect, this ferumoxtran enhancement occurred clearly in areas of increased T2 signal intensity in the white matter, where 26 days before no gadolinium enhancement was seen. However, the solid tumor demonstrated less ferumoxtran enhancement than gadolinium enhancement. Ferumoxtran does not cross the intact BBB even in much higher doses with intraarterial administration (15). Three possibilities or a combination thereof may account for this phenomenon. First, an accumulation mechanism may exist for ferumoxtran but not for gadolinium. Second, ferumoxtran may extend from gadolinium-enhancing to non–gadolinium-enhancing regions by means of diffusion (less likely), convection, and/or intracellular transport (more likely) (15). Third, ferumoxtran may cross the endothelium by a distinct mechanism other than the intercellular junctions in these regions. Animal studies and/or larger patient series will be needed to address this issue.

The other previously mentioned finding that requires further evaluation is the intensive peripheral ferumoxtran accumulation rather than accumulation in the center of tumor. In assessing invasive breast cancer, Harms et al (29) also reported the accumula-

tion of ferumoxtran primarily in the reactive cells at the tumor–normal tissue interface at histologic and MR imaging examinations of the breast as we did at our histologic and MR imaging examinations of brain (Fig 3).

In all of the ferumoxtran-enhanced tumors, the tumor margins were sharp without detectable difference in sharpness on the 6- or 24-hour ferumoxtran-enhanced images. This observation is in agreement with the study of Enochs et al (17). Both the gadolinium chelate and USPIO particles can extravasate and accumulate in the tumoral interstitium; however, the gadolinium chelate will diffuse over time into the surrounding brain to a much greater degree than will ferumoxtran, presumably owing to the larger size, decreased diffusion coefficient, and cellular uptake of ferumoxtran. Long-lasting as well as better delineation of the tumor with ferumoxtran, in contrast to the gadolinium chelate, raises the possibility of the application of this iron oxide particle for preoperative and intraoperative surgical planning and postoperative assessment of surgical resection. Indeed, it is intriguing that in an animal model by Knauth et al (30), intravenously administered monocrystalline iron oxide nanoparticles (MION) did not cause high signal intensity on T1-weighted images in the normal or the postoperative brain after superficial electrocoagulation or deep ablation, which is a problem with gadolinium chelates. Gadolinium enhancement caused by surgical BBB damage makes it difficult to correctly differentiate between residual tumor and postoperative enhancement. This difference may make ferumoxtran especially useful for intraoperative or postoperative MR imaging to assess the degree of resection.

Finally, virus-mediated gene therapy is a promising treatment for brain tumors. Delivery of viruses across the BBB to the tumor and brain around the tumor is one of the major obstacles; however, direct interstitial instillation and systemic infusion with BBB disruption have been proposed (15). Preclinical studies have been carried out with MION, which is the preclinical grade preparation of ferumoxtran. According to the results of studies with the co-injection of adenovirus and MION (with BBB disruption or intracerebral inoculation), it appears that the volume of distribution is very similar (31). Intracellular MION has already been detected in rodent neurons and pericytes by electron microscopy after intraarterial administration, with BBB disruption (15, 16). Similarly, intracellular adenovirus has been demonstrated by immunostaining for transgenic protein expression after intraarterial administration, with BBB disruption (31). The current study showed that intravenously administered viral-sized USPIO particles do accumulate in tumors, and they were demonstrated histologically in the tumor and in the tumor-brain interface both intracellularly and interstitially (Fig 3G and H). Because the size of the USPIO particles is similar to the size of small viruses and both USPIO and adenovirus have been demonstrated intracellularly, these iron oxide particles may serve as an important model to evaluate potential transvascular as well as interstitial vector delivery.

## Conclusion

We showed that ferumoxtran, in contrast to ferumoxides, can be used as an intravenous contrast agent for MR imaging of intracranial tumors; however, its utility in brain tumor imaging needs further study. Enhancement with ferumoxtran was comparable to but more variable than that with the gadolinium chelate, and previous radiation therapy may have an effect on ferumoxtran accumulation. All of the malignant tumors showed ferumoxtran enhancement, but more studies are needed to determine the degree of ferumoxtran accumulation in low-grade gliomas. For intraaxial tumors, ferumoxtran enhancement seems to be dependent on both the degree of BBB incompetency and the number of parenchymal cells within and around the tumor able to trap it. For extra-axial tumors, which do not have a BBB, ferumoxtran accumulation (enhancement) may mainly depend on the presence of parenchymal cells capable of taking up the iron particles, though altered vascular endothelium secondary to radiation therapy may also be a factor. Histologic examination showed similar distribution of the ferumoxtran particles as seen on MR images, that is, primarily at the tumor margin, with less central localization. Also, the intratumoral demonstration of ferumoxtran after intravenous administration may enable this iron oxide particle to be used as a marker for viral vector delivery in malignant brain tumors. The changes of increase in signal intensity on the 24-hour ferumoxtran-enhanced images compared with that of the 6-hour images better delineate iron accumulation and decrease the blood-pool effect, although extending that to 48 or 72 hours (two or three half-lives) may further increase this effect. As expected, the most striking signal intensity changes could be observed on the SE T1- and GRE T2*-weighted images, suggesting these sequences might be the best to evaluate iron accumulation. In addition, ferumoxtran signal intensity changes that persist for at least 24 hours may render advantages over gadolinium enhancement for intraoperative MR imaging as well as postoperative assessment of surgical resection.

## Acknowledgment

Ferumoxtran-10 (Combidex) was kindly provided by Advanced Magnetics, Cambridge, MA.

## References

1. Hagspiel KD, Neidl KFW, Eichenberger AC, et al. **Detection of liver metastasis: comparison of superparamagnetic iron oxide-enhanced and unenhanced MR imaging at 1.5 T with dynamic CT, intraoperative US, and percutaneous US.** *Radiology* 1995;196:471–478
2. Reimer P, Tombach B. **Hepatic MR with SPIO: detection and characterization of focal liver lesions.** *Eur Radiol* 1998;8:1198–1204
3. Mergo PJ, Engelken JD, Helmberger T, Ros PR. **MRI in focal liver disease: a comparison of small and ultra-small superparamagnetic**

**iron oxide as hepatic contrast agents.** *J Magn Reson Imaging* 1998; 8:1073–1078
4. Saini S, Sharma R, Baron RL, et al. **Multicenter dose-ranging study on the efficacy of USPIO ferumoxtran-10 for liver MR imaging.** *Clin Radiol* 2000;55:690–695
5. Weissleder R, Hahn PF, Stark DD, et al. **Superparamagnetic iron oxide: enhanced detection of focal splenic tumors with MR imaging.** *Radiology* 1998;169:399–403
6. Harisinghani MG, Saini S, Slater GJ, et al. **MR imaging of pelvic lymph nodes in primary pelvic carcinoma with ultrasmall superparamagnetic iron oxide (Combidex): preliminary observations.** *J Magn Reson Imaging* 1997;7:161–163
7. Nguyen BC, Stanford W, Thompson BH, et al. **Multicenter clinical trial of ultrasmall superparamagnetic iron oxide in the evalution of mediastinal lymph nodes in patients with primary lung carcinoma.** *J Magn Reson Imaging* 1999;10:468–473
8. Hoffman HT, Quets J, Toshiaki T, et al. **Functional magnetic resonance imaging using iron oxide particles in characterizing head and neck adenopathy.** *Laryngoscope* 2000;110:1425–1430
9. Taylor AM, Panting JR, Keegan J, et al. **Safety and preliminary findings with the intravascular contrast agent NC100150 injection for MR coronary angiography.** *J Magn Reson Imaging* 1999;9:220–227
10. Anzai Y, Prince MR, Chenevert TL, et al. **MR angiography with an ultrasmall superparamagnetic iron oxide blood pool agent.** *J Magn Reson Imaging* 1997;7:209–214
11. Bonnemain B. **Superparamegetic agents in magnetic resonance imaging: physicochemical characterisitics and clinical applications: a review.** *J Drug Target* 1998;6:167–174
12. Xu S, Jordan Ek, Brocke S, et al. **Study of relapsing remitting experimental allergic encephalomyelitis SJL mouse model using MION-46L enhanced in vivo MRI: early histopathological correlation.** *J Neurosci Res* 1998;52:549–558
13. Dousset V, Delalande C, Ballarino L, et al. **In vivo macrophage activity imaging in the central nervous system detected by magnetic resonance.** *Magn Reson Med* 1999;41:329–333
14. Dousset V, Ballarino L, Delalande C, et al. **Comparison of ultrasmall particles of iron oxide (USPIO)-enhanced T2-weighted, conventional T2-weighted, and gadolinium-enhanced T1-weighted MR images in rats with experimental autoimmmune encephalomyelitis.** *AJNR Am J Neuroradiol* 1999;20:223–227
15. Neuwelt EA, Weissleder R, Nilaver G, et al. **Delivery of virus-sized iron-oxide particles to rodent CNS neurons.** *Neurosurgery* 1994;34: 777–784
16. Muldoon LL, Pagel MA, Kroll RA, Roman-Goldstein S, Jones RS, Neuwelt EA. **A physiological barrier distal to the anatomic blood-brain barrier in a model of transvascular delivery.** *AJNR Am J Neuroradiol* 1999;20:217–222
17. Enochs WS, Harsh G, Hochberg F, Weissleder R. **Improved delineation of human brain tumors on MR images using a long-circulating, superparamagnetic iron oxide agent.** *J Magn Reson Imaging* 1999;9:228–232
18. Egelhof T, Delbeck N, Hartmann M, et al. **Can superparamagnetic contrast media improve MRI-tomographic images of experimental gliomas?** *Radiologe* 1998;38:943–947
19. Zimmer C, Weissleder R, Poss K, Bogdanova A, Wright SC Jr, Enochs WS. **MR imaging of phagocytosis in experimental gliomas.** *Radiology* 1995;197:533–538
20. Moore A, Marecos E, Bogdanov A Jr, Weissleder R. **Tumoral distribution of long-circulating dextran-coated iron oxide nanoparticles in a rodent model.** *Radiology* 2000;214:568–574
21. Weissleder R, Cheng HC, Bogdanova A, Bogdanov A Jr. **Magnetically labeled cells can be detected by MR imaging.** *J Magn Reson Imaging* 1997;7:258–263
22. Kroll RA, Pagel MA, Muldoon LL, Neuwelt EA. **Increasing volume of distribution to brain with interstitial infusion: dose, rather than convection, may be the most important factor.** *Neurosurgery* 1996;38:746–754
23. Remsen LG, McCormick CI, Roman-Goldstein S, et al. **MR of carcinoma-specific monoclonal antibody conjugated to monocrystalline iron oxide nanoparticles: the potential for noninvasive diagnosis.** *AJNR Am J Neuroradiol* 1996;17:411–418
24. Jung C, Jacobs P. **Physical and chemical properties of superparamagnetic iron oxide MR contrast agents: ferumoxides, ferumoxtran, ferumoxsil.** *Magn Reson Imaging* 1995;13:661–674
25. Kroll RA, Neuwelt EA. **Outwitting the blood-brain barrier for therapeutic purposes: osmotic opening and other means.** *Neurosurgery* 1998;42:1083–1100
26. Kraemer DF, Fortin D, Doolittle ND, Neuwelt EA. **Association of total dose intensity of chemotherapy in primary CNS lymphoma (human non-AIDS) and survival.** *Neurosurgery* 2001;48:1033–1041
27. Barnett PA, Roman-Goldstein S, Ramsey F, et al. **Differential permeability and quantitative MR imaging of a human lung carcinoma brain xenograft in the nude rat.** *Am J Path* 1995;146:436–449
28. Remsen LG, McCormick CI, Sexton G, et al. **Long-term toxicity and neuropathology associated with the sequencing of cranial irradiation and enhanced chemotherapy delivery.** *Neurosurgery* 1997; 40:1034–1042
29. Harms SE, Hinton T, Manning L, Korourian S. **New MRI contrast agent for labeling of tumor-associated macrophages that stimulate tumor angiogenesis (abstr).** In: *Proceedings of the Eighth Meeting of the International Society for Magnetic Resonance in Medicine 2000.* Berkeley, Calif: International Society for Magnetic Resonance in Medicine, 2000;616
30. Knauth M, Egelhof T, Roth SU, Wirtz CR, Sartor K. **Monocrystalline iron oxide nanoparticles: possible solution to the problem of surgically induced intracranial contrast enhancement in intraoperative MR imaging.** *AJNR Am J Neuroradiol* 2001;22:99–102
31. Muldoon LL, Nilaver G, Kroll RA, et al. **Comparison of intracerbral inoculation and osmotic blood-brain barrier disruption for delivery of adenovirus, herpesvirus and iron oxide particles to normal rat brain.** *Am J Pathol* 1995;147:1840–1851